Int J Thermophys (2010) 31:187–198
DOI 10.1007/s10765-009-0590-6

Thermal Transport Properties of $Cd_{1-x}Mg_xSe$ Mixed Crystals Measured by Means of the Photopyroelectric Method

M. Pawlak · F. Firszt · S. Łęgowski · H. Męczyńska · J. Gibkes · J. Pelzl

Received: 21 April 2009 / Accepted: 7 May 2009 / Published online: 10 July 2009

Abstract The concentration dependence of the thermal conductivity and thermal diffusivity were determined for $Cd_{1-x}Mg_xSe$ mixed crystals in the temperature range between 20 °C and 40 °C. To determine the thermal transport properties, the photopyroelectric setup in the back detection configuration was constructed. In the concentration range $0 < x < 0.36$, both thermal conductivity and thermal diffusivity were found to decrease with increasing magnesium concentration as well as with increasing temperature. The observed concentration dependence is discussed in the framework of the Adachi model.

Keywords CdMgSe mixed crystals · Photopyroelectric technique · Thermal conductivity · Thermal diffusivity · Thermal resistivity

1 Introduction

CdSe-based semiconducting compounds and their heterostructures have potential application in optoelectronics. $Cd_{1-x}Mg_xSe$ alloys are considered to be promising for the fabrication of full color visible optical devices, because bandgap energies of CdSe and MgSe are 1.74 eV and about 4 eV, respectively [1]. Green-light emitting structures using n-CdSe, p-ZnTe, $Cd_{1-x}Mg_xSe$, and $Zn_{1-x}Mg_xTe$ layers have been already successfully constructed [2]. The room-temperature ZnCdSe/ZnCdMgSe photo-pumped

M. Pawlak (✉) · J. Gibkes · J. Pelzl
Experimental Physics III, Ruhr-University Bochum,
Universitaetsstrasse 150, NB 3/170, 44780 Bochum, Germany
e-mail: mispawlak@yahoo.pl

F. Firszt · S. Łęgowski · H. Męczyńska
Institute of Physics, Nicolaus Copernicus University, Grudziądzka 5/7, Toruń, Poland

quantum well blue–green laser was also fabricated [3], which implies that these new materials have important applications. Photothermal methods have become a very useful tool for measurements of the thermal parameters of semiconductors. The significance of thermal phenomena becomes more and more important because of the problem of energy dissipation in miniaturized semiconducting devices. Thermal diffusivity is a very important physical parameter in device modeling. It is a unique parameter for each material, strongly dependent on the composition, and structural characteristic of the sample.

2 Experimental

2.1 Samples

$Cd_{1-x}Mg_xSe$ single crystals were grown by the high-pressure Bridgman method without a seed under an argon overpressure [4]. The mixture of CdSe and metallic Mg was put into a graphite crucible. The purity of CdSe and Se reaction components was 6 N, and that of Mg was 99.8 %. The temperature of the heating zone was kept at (1880 ± 0.5) K. The crucible was held at that temperature for 2 h and then moved out from the heating zone with a lowering speed of 4.2 mm·h^{-1}. The obtained crystals were cylinders with raw dimensions of 8 mm to 10 mm in diameter and 40 mm to 50 mm in length. The crystals have a longitudinal gradient of magnesium concentration (Mg content increases from the tip to the end of the crystal). For a crystal with $x = 0.3$, the Mg concentration gradient is about 0.01 cm^{-1}. The crystals exhibit the wurtzite structure. The lattice constant of $Cd_{1-x}Mg_xSe$ crystals decreases with increasing Mg content [5]. The crystals were cut perpendicular to the growth direction into 0.9 mm to 1.5 mm thick plates. Next the plates were mechanically polished and chemically etched in a mixture of $K_2Cr_2O_7$, H_2SO_3, and H_2O in the proportion 3:2:1. Then they were treated in CS_2 and a hot 50 % NaOH solution and finally rinsed in water and ethyl alcohol.

2.2 PPE Signal

The average temperature oscillation T_p at angular frequency ω_0 in a pyroelectric detector leads to variations of the surface charge density Q due to the pyroelectric effect and can be expressed as [6]

$$Q(\omega_0) = p\left\langle T_p(\omega_0)\right\rangle, \tag{1}$$

where p is the pyroelectric coefficient of the detector. Time-dependent variations of the surface charge cause a current flow through the detector of thickness L_p [7,8];

$$I(\omega_0) = A\frac{d\langle Q(\omega_0)\rangle}{dt} = pA\frac{d\left\langle T_p(\omega_0)\right\rangle}{dt} = pA\left(\frac{1}{L_p}\int_{L_p} T_p(x,\omega_0)dx\right)\frac{d}{dt}e^{i\omega_0 t}$$
$$= ipA\omega_0\theta_p(\omega_0)\,e^{i\omega_0 t}, \tag{2}$$

where A is the transducer area and $\theta_{\mathrm{p}}(\omega_0) = \frac{1}{L_{\mathrm{p}}}\int_{L_{\mathrm{p}}} T_{\mathrm{p}}(x,\omega_0)\mathrm{d}x$. $T_{\mathrm{p}}(\omega_0, x)$ is the temperature field in the pyroelectric detector. In our experimental configuration, we can apply the following model of a sample: one surface (front) was covered by a 20 μm to 30 μm thick graphite layer which prevents exciting light to penetrate the sample. The other (rear) was connected to the detector which monitored the thermal wave transmitted through the sample. The distribution of the thermal wave is the solution of one-dimensional thermal transport equations as a result of heat conduction through the sample. Similar theoretical models were considered by Chirtoc and Mihalescu [9] and Mandelis and Zver [7]. In both cases the influence of the thermal interface between the rear surface of the sample and the detector was neglected. Experimentally a good thermal interface was achieved with a very thin grease layer. In our measurements, the thermal waves are generated by surface heating. As the thermal thickness of the graphite surface layer is small, its contribution to the heat transport problem is neglected. Also, the thermal contact of the sample to the detector by the grease layer is considered to be ideal. However, Salazar [10] demonstrated that in some cases the thermal diffusivity α of the sample is underestimated due to the influence of the grease layer. He calculated the error of the α estimation in the presence of about a 2 μm to 3 μm thick grease layer. He found that the error is large for thin and good thermal conductors at high frequencies and decreases with increasing thickness and decreasing thermal diffusivity of a material and modulation frequencies. Although in our measurements we used a different grease, one can deduce that the investigated samples as well as a glassy carbon are rather poor thermal conductors. Furthermore, this effect is additionally reduced because measurements were performed at modulated low frequencies. Therefore, the temperature field in the case of when the sample and the detector are both thermally thick and optically opaque using a formula of Chirtoc and Mihalescu [9] and Mandelis and Zver [7] is expressed as

$$\Theta_{\mathrm{p}}(\omega_0) = \left(\frac{\eta_{\mathrm{s}}\alpha_{\mathrm{p}}}{k_{\mathrm{p}}\left(1+\frac{k_{\mathrm{s}}\sqrt{\alpha_{\mathrm{p}}}}{k_{\mathrm{p}}\sqrt{\alpha_{\mathrm{s}}}}\right)\omega_0}\right)\exp\left(-\sqrt{\frac{\omega_0}{2\alpha_{\mathrm{s}}}}L_{\mathrm{s}}\right)\exp\left(-i\left(\frac{\pi}{2}+\sqrt{\frac{\omega_0}{2\alpha_{\mathrm{s}}}}L_{\mathrm{s}}\right)\right), \quad (3)$$

where η_{s} is the nonradiative conversion efficiency for an absorbing sample which is characterized by thickness L_{s}, thermal diffusivity α_{s},and thermal conductivity k_{s}. The detector is characterized by thermal diffusivity α_{p} and thermal conductivity k_{p}. Therefore, the PPE signal is given by

$$I(\omega_0) = (pI_0A)\left[\frac{\eta_{\mathrm{s}}\alpha_{\mathrm{p}}}{k_{\mathrm{p}}(1+b_{\mathrm{sp}})}\right]\exp\left(-\sqrt{\frac{\omega_0}{2\alpha_{\mathrm{s}}}}L_{\mathrm{s}}\right)\exp\left[-\mathrm{i}\left(\frac{\pi}{2}+\sqrt{\frac{\omega_0}{2\alpha_{\mathrm{s}}}}L_{\mathrm{s}}\right)\right], \quad (4)$$

where I_0 is the intensity of the optical excitation and the PPE phase is given by

$$\phi = -\frac{\pi}{2} - \sqrt{\frac{\pi f}{\alpha_{\mathrm{s}}}}L_{\mathrm{s}} = -\frac{\pi}{2} - m\sqrt{f}. \quad (5)$$

The coefficient m can be easily determined from experimental data. If the sample's thickness is known, then the thermal diffusivity is given by

$$\alpha_s = \frac{\pi L_s^2}{m^2}. \tag{6}$$

Additionally the PPE amplitude can be written as

$$\ln\left(I\left(\omega_0\right)\right) = B + \left(-\sqrt{\frac{L_s^2}{2\alpha_s}}\right)\sqrt{\omega_0} = B - \sqrt{\frac{\pi L_s^2}{\alpha_s}}\sqrt{f} = B - m\sqrt{f}, \tag{7}$$

where $B = \ln\left[\frac{pI_0A\eta_s\alpha_p}{k_p\left(1+\frac{k_s\sqrt{\alpha_p}}{k_p\sqrt{\alpha_s}}\right)}\right]$.

2.3 Experimental Setup

The PPE measurements are performed in the back detection configuration, where the heat is generated on the front side of the sample and the temperature oscillations are measured with the pyroelectric detector contacted to the back side of the sample. The experimental setup constructed for the back detection configuration is presented in Fig. 1. The thermal waves are excited by an argon ion laser with an output power of 200 mW and operating wavelength $\lambda = 514$ nm. The laser beam of about 1.89 mm diameter was intensity modulated by means of an acousto–optical modulator in the frequency range from 1 Hz to 10 Hz and focused onto the sample. The front surface of the sample was covered by an optically opaque 20 μm to 30 μm graphite coating. Samples were attached to a pyroelectric detector by means of a grease layer (Apiezon T grease). As the grease layer was very thin, its contribution to the PPE signal could

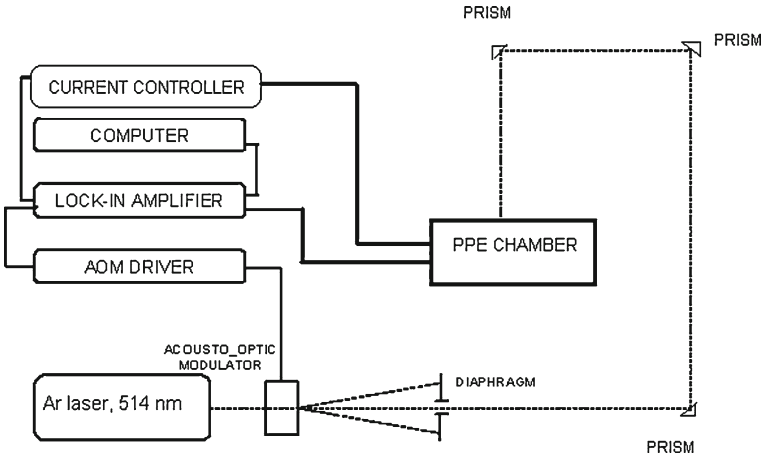

Fig. 1 PPE experimental setup

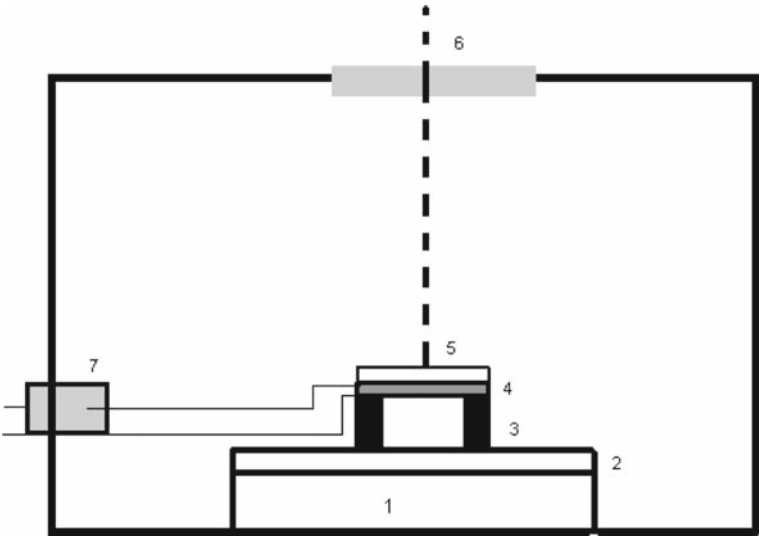

Fig. 2 PPE chamber: 1—Peltier element, 2—aluminum support, 3—cylindrical cooper support, 4—PZT detector, 5—sample with optically opaque cover layer, 6—quartz window, 7—BNC connector for PPE signal

be neglected. A 0.98-mm thick lead zirconate titanate PZT crystal was used as a pyroelectric detector. The PPE signal detection was performed by means of a lock-in amplifier (Stanford 830). The detector was placed on a cooper plate with a drilled hole (inside was air). The sample–detector–copper support assembly was placed in an aluminum chamber. A schematic of the PPE chamber is presented in Fig. 2.

The temperature was varied in the range from 20 °C up to 40 °C by means of a Peltier element which was driven by a homemade current controller. Figure 3a shows the PPE phase from the detector alone as a function of the modulation frequency in the temperature range from 26 °C to 36 °C. Error bars for PPE phases were approximately 1.5°. From the experimental data in Fig. 3a, one can see that in the investigated range of the temperature the PPE phases remain constant within the error bars. This means that the thermal properties of the detector can be assumed constant under our measurement conditions. We had also observed small changes in the PPE amplitudes, but these can be caused by the temperature dependence of the pyroelectric coefficient and/or thermal effusivity $e_p(e_p = k_p(\alpha_p)^{-1/2})$ of the PZT detector as well as long-term fluctuations of the laser intensity. These effects can be minimized by an appropriate normalization procedure. Detenclos et al. [11] normalized the PPE signal from an investigated material to the one obtained with the detector alone or to the signal obtained with a reference sample. They considered the PPE signal for the sample and the detector both thermally thick and optically opaque and pointed out that the normalized signal is not influenced by the temperature dependence of the pyroelectric coefficient; hence, only a knowledge of the thermal effusivity of the detector is required. In fact, we normalized our experimental data to the reference sample instead of the detector alone as the absorption of laser light at the detector electrode is different from that in the graphite layer [11]. In addition, it is also possible that the heating spot

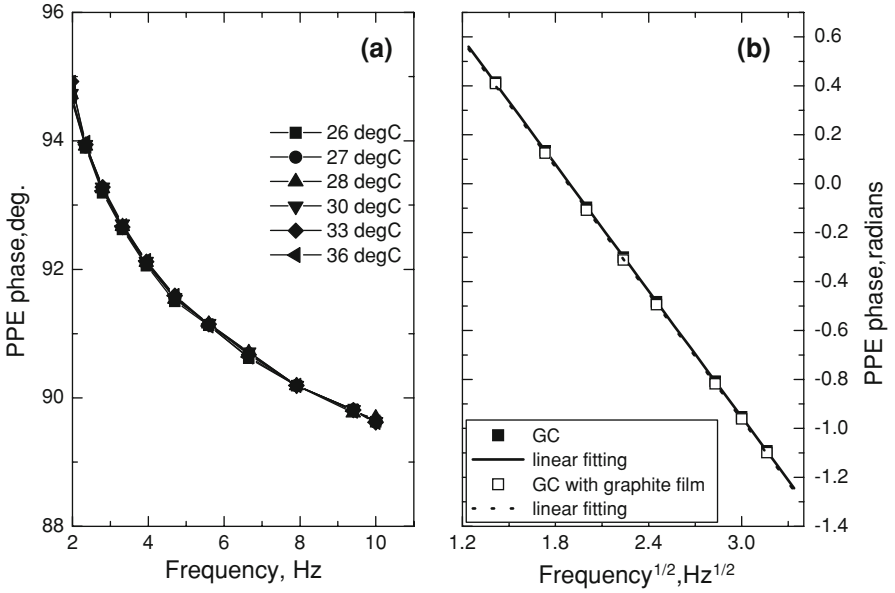

Fig. 3 PPE phases of (**a**) the detector at different temperatures (in °C) and (**b**) glassy carbon as a function of the modulation frequency. Fit of the experimental PPE phase of glassy carbon (•) and glassy carbon with graphite film (■) with Eq. 5 yields the same value $m = -0.860 \pm 0.003$ for both

(laser beam spot) interacts (energy exchange) with silver contacts on the surface of the detector, and this could lead to a worse signal-to-noise ratio (SNR) than in the case of normalization to a reference material.

As a reference sample, a 0.98 mm thick piece of a glassy carbon (Type G) was used. Figure 3b presents the PPE phases at room temperature of the glassy carbon as a function of the square root of the modulation frequency. It is worthwhile to note that the error bars were approximately 0.5°. Using Eqs. 5 and 6, the thermal diffusivity from the as-measured PPE phases of the glassy carbon was estimated to be $4.22 \times 10^{-6}\,\mathrm{m}^2 \cdot \mathrm{s}^{-1}$. The same value of the thermal diffusivity was obtained from the as-measured PPE amplitudes by Eqs. 7 and 6. The specific heat capacity C in the temperature range from 20 °C to 40 °C was determined from differential scanning calorimetry (DSC) measurements, and it was found that the specific heat capacity C is about $1050\,\mathrm{J} \cdot \mathrm{kg}^{-1} \cdot \mathrm{K}^{-1}$ within the error limit (3 % to 5 %) that is constant in the covered temperature range. Using the literature value (http://www.htw-gmbh.de/) of the mass density $\rho = 1.42 \times 10^3\,\mathrm{kg} \cdot \mathrm{m}^{-3}$, the thermal conductivity of the glassy carbon type G was calculated to be $6.3\,\mathrm{W} \cdot \mathrm{m}^{-1} \cdot \mathrm{K}^{-1}$, which is in excellent agreement with the value deduced from the data sheet of the producer of the glassy carbon (http://www.htw-gmbh.de/). This demonstrates the reliability of the present experimental setup and measurement procedure for the experimental determination of the thermal diffusivity.

Unlike the black glassy carbon, the investigated semiconductor samples have smaller absorption coefficients β; thus, the light can penetrate deeper into the sample producing heat sources also in the subsurface regions. For this reason a thin black graphite layer was deposited on the surface. The advantage of an optically opaque cover layer at

the present experimental conditions (514 nm laser) was that it avoids a super-bandgap excitation that creates photocarriers which can act as scattering centers for phonons. This scattering affects the thermal transport properties (decreasing k) of investigated semiconductors. These phenomena could complicate the experimental data interpretation. Figure 3b shows the effect of the graphite cover layer on the raw PPE phases from the glassy carbon. It is clearly seen that this layer does not affect the PPE phase. The same value of the coefficient m was obtained for PPE amplitudes. Therefore, the thermal diffusivity can be calculated from the as-measured PPE phases and amplitudes in the presence of the graphite coating in the same way as for the glassy carbon sample.

3 Experimental Results and Discussion

Figure 4 shows experimental phase lags of investigated mixed semiconductors as a function of the square root of the modulation frequency. The thermal diffusivities reported in Table 1 were calculated using Eq. 6 by fitting the as-measured PPE phases with Eq. 5. The thermal-diffusivity values could be confirmed by using Eq. 6 but with the coefficient m fitted from the as-measured PPE amplitudes by Eq. 7. With increasing magnesium concentration, the thermal diffusivity decreases markedly. Figure 5 shows experimental data and theoretical curves of the temperature dependence of thermal diffusivities for the investigated crystals. The fits assume a linear temperature variation $\alpha(T) = aT$. It is clearly seen that with increasing temperature the thermal diffusivity for all investigated crystals decreases. The steepness of this slope decreases with

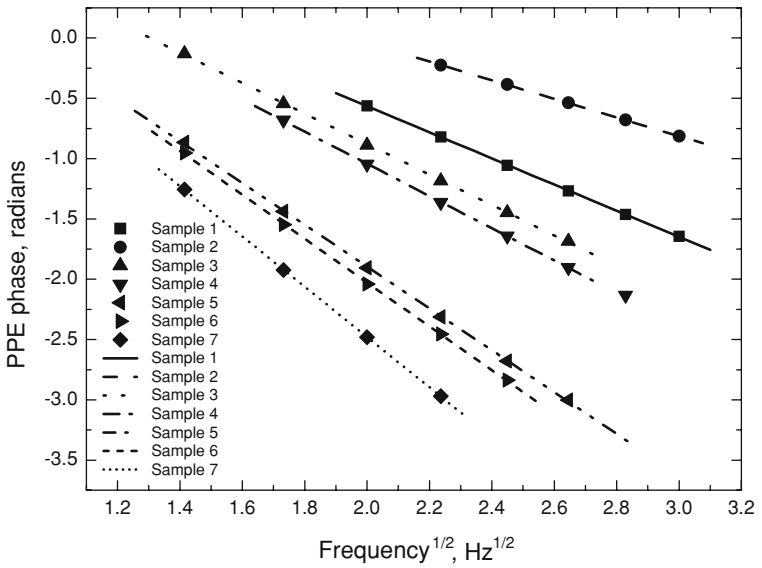

Fig. 4 Experimental PPE phase lags (*scatters*) of the investigated crystals with linear fits (*lines*) versus square root of the modulation frequency. Fitting parameters are reported in Table 1

Table 1 Results of linear fits to Eq. 5 and calculated values of the thermal diffusivities of $Cd_{1-x}Mg_xSe$ mixed crystals from Eq. 6

Sample	Magnesium concentration, x (mole fraction)	Thickness, L (mm)	m	α ($10^{-6}\,m^2 \cdot s^{-1}$)
1	0.00	1.325	−1.08	4.73
2	0.00	0.923	−0.77	4.48
3	0.06	1.043	−1.26	2.15
4	0.14	1.306	−1.79	1.67
5	0.15	0.944	−1, 34	1.58
6	0.33	1.174	−1.85	1.26
7	0.36	1.294	−2.12	1.17

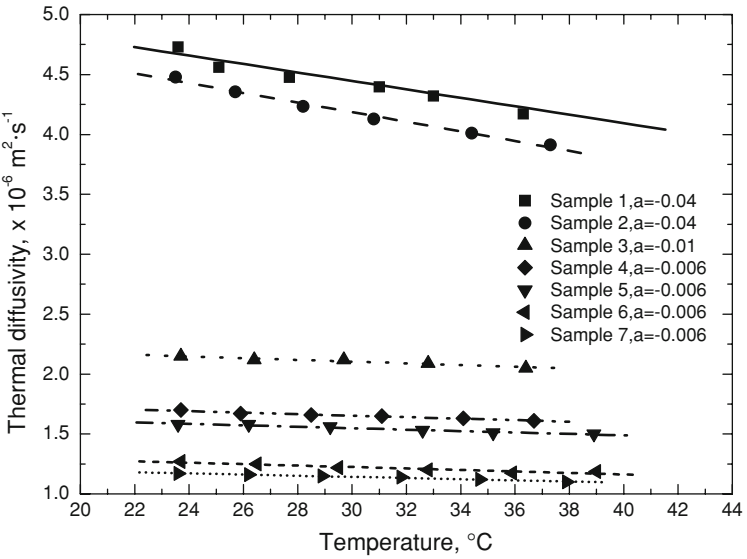

Fig. 5 Temperature dependence of the thermal diffusivity for the investigated crystals fitted with a linear temperature dependence $\alpha(T) = aT$

increasing magnesium concentration. The obtained values of thermal diffusivities for investigated crystals from raw PPE phases and amplitudes were substituted in the normalized PPE amplitude $S_n(f)$ (divided amplitude of a sample by the reference sample) to determine the thermal conductivities. The nonlinear data-fitting procedure relied on minimizing the following expression in a least-squares sense:

$$\frac{1}{2}\sum_{i=1}^{N}\left(F\left(k_s, f_i\right) - S_n\left(f_i\right)\right)^2 \tag{8}$$

Only one parameter (thermal conductivity k_s) was applied. $F(k_s, f_i)$ is the theoretical PPE amplitude (and normalized by the theoretical response of the PPE amplitude

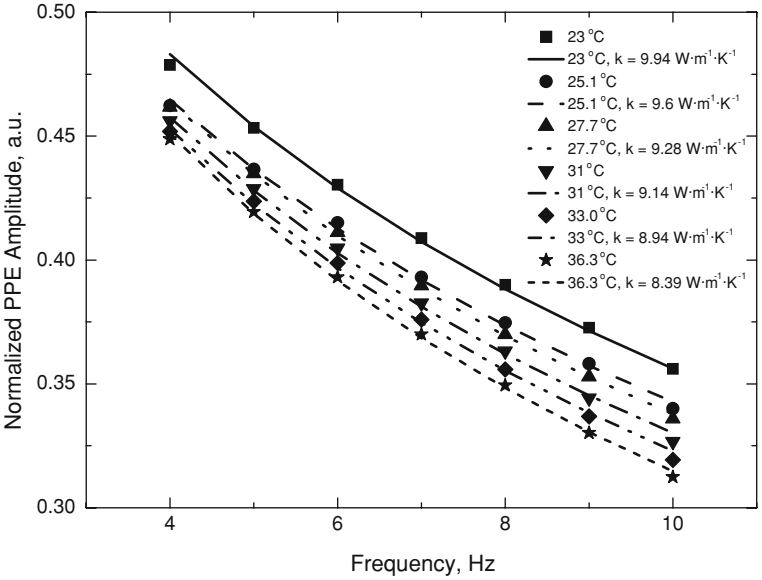

Fig. 6 Best fits (*lines*) to the normalized PPE amplitude (*scatters*) of sample 1 at different temperatures

of the glassy carbon) described by Eq. 4, and N is the number of experimental points. The nonlinear data fitting was based on the built-in MATLAB function LSQCURVEFIT. The following parameters were used during the fitting procedure for a pyroelectric detector: $k_p = 1.13\,\mathrm{W \cdot m^{-1} \cdot K^{-1}}$ and $\alpha_p = 4.95 \times 10^{-7}\,\mathrm{m^2 \cdot s^{-1}}$, and for the glassy carbon, $k_s = 6.3\,\mathrm{W \cdot m^{-1} \cdot K^{-1}}$ and $\alpha_s = 4.22 \times 10^{-6}\,\mathrm{m^2 \cdot s^{-1}}$. It was assumed that the temperature dependence of the thermal conductivity of the glassy carbon results only from that of the thermal diffusivity as determined from the PPE phases. Figure 6 shows the best fits to the normalized PPE amplitude for sample 1. It is clearly seen that with increasing temperature the thermal conductivity for sample 1 decreases. For the temperature 27.7 °C (300.7 K) the thermal conductivity of sample 1 (CdSe) is $9.28\,\mathrm{W \cdot m^{-1} \cdot K^{-1}}$. This value is in good agreement with the thermal conductivity of the CdSe ($9\,\mathrm{W \cdot m^{-1} \cdot K^{-1}}$) crystal obtained by [12]. Additionally, for single crystals, the thermal conductivity may depend on crystallographic directions as in the case of ZnO [12]. Although, our samples were not oriented, this effect can be neglected because measurements were performed at high temperatures.

The frequency-dependent normalized amplitude obtained at different temperatures from the other samples have been fitted in the same way. The best results for all crystals of the fitting procedure are shown in Table 2 and Fig. 7. Figure 7 presents the temperature dependence of the thermal conductivity for $Cd_{1-x}Mg_xSe$ mixed crystals with different magnesium concentrations. The dynamics of these changes can be expressed by coefficient n extracted from $k(T) = aT^n$ on log–log scales. Values of the coefficient n are presented in Fig. 7. Obviously, n is nearly constant for all investigated crystals within the error limit of the fitting (± 0.05). The electron contribution to the thermal conductivity can be calculated for a degenerate semiconductor (because carrier concentrations of investigated crystals are high) from a formula given by [13]

Table 2 Thermal conductivity of $Cd_{1-x}Mg_xSe$ mixed crystals at room temperature resulting from the best fits using MATLAB

Sample	Magnesium concentration, x (mole fraction)	Thickness L (mm)	k ($W \cdot m^{-1} \cdot K^{-1}$)	Electrical conductivity ($\Omega^{-1} \cdot m^{-1}$)	k_e ($W \cdot m^{-1} \cdot K^{-1}$)
1	0.00	1.325	9.28	1000	0.007
2	0.00	0.923	–	–	–
3	0.06	1.043	5.34	–	–
4	0.14	1.306	3.82	1200	0.009
5	0.15	0.944	3.93	–	–
6	0.33	1.174	3.13	500	0.004
7	0.36	1.294	3.00	–	–

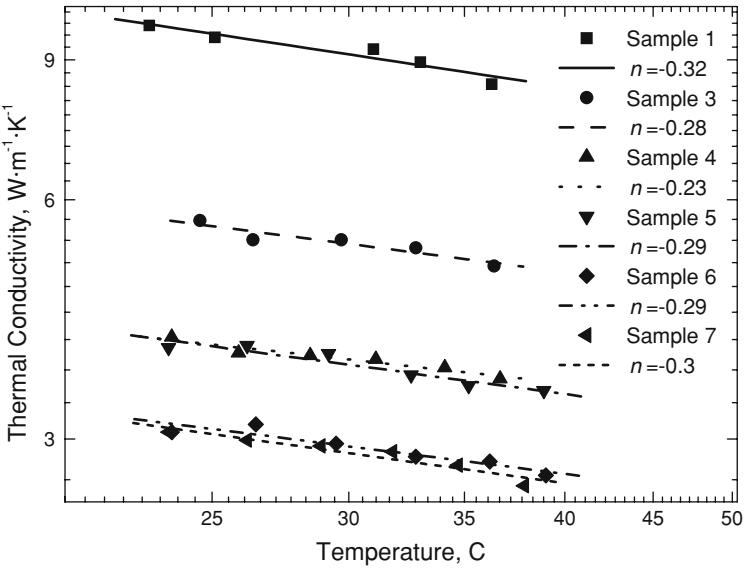

Fig. 7 Temperature dependence of the thermal conductivity (*scatters*) for $Cd_{1-x}Mg_xSe$ mixed crystals with different Mg concentrations and the best fits (*lines*) to $k(T) = aT^n$ on log–log scale

$$k_e = \left(\frac{k_b}{e}\right)^2 \sigma_e L T, \tag{9}$$

where T is the temperature, e is the elementary charge, and k is the Boltzmann constant. The electrical conductivity σ_e for samples 1, 4, and 6 were taken from Hall measurements [14] and the Lorenz factor was assumed to be $\pi^2/3$. The obtained results are shown in Table 2. Because the electron contribution to the thermal conductivity is very small, the heat is carried by phonons. This behavior is expected for CdSe crystals at room temperature [12]. Therefore, the thermal conductivity can be related only to the lattice; hence, the thermal resistivity can be introduced as the inverse of the (lattice)

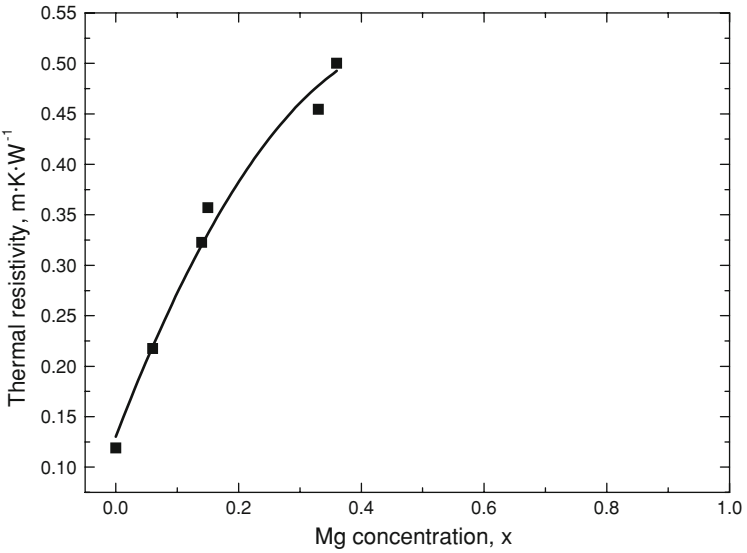

Fig. 8 Reciprocal thermal conductivity (thermal resistivity) of the $Cd_{1-x}Mg_xSe$ mixed crystals as a function of magnesium concentration at room temperature

thermal conductivity. Figure 8 presents the thermal resistivity W as a function of the magnesium concentration at room temperature. The thermal resistivity W increases with increasing magnesium concentration. This behavior is expected when large numbers of magnesium atoms are added to the host lattice, and they act as scattering centers for phonons. A similar behavior of the thermal resistivity was found by Adachi [15] in III–V semiconductors. He gave the expression of the thermal resistivity as a function of concentration x [15] as

$$W(x) = x\,W_{\mathrm{CdSe}} + (1-x)\,W_{\mathrm{MgSe}} + C_{\mathrm{Cd-Mg}}x\,(1-x), \tag{10}$$

where W_{CdSe} and W_{MgSe} are the thermal resistivities of CdSe and MgSe, respectively. The coefficient $C_{\mathrm{Cd-Mg}}$ is called a nonlinear parameter, and it is a contribution arising from the lattice disorder generated in the ternary $Cd_{1-x}Mg_xSe$ system by random distribution of Cd and Mg atoms in one of the two sublattice sites [15]. In Fig. 8 the best fit (line) to Eq. 10 is also shown. The nonlinear parameter was found to be $1.59\,\mathrm{W\cdot m^{-1}\cdot K^{-1}}$, while the thermal conductivity of MgSe was $7.69\,\mathrm{W\cdot m^{-1}\cdot K^{-1}}$.

Although, MgSe does not exist in nature, the value obtained from fitting is rather unexpected. This can be explained because the Adachi model is a simplification of the Abeles model [16]. Adachi had taken into account only strain scattering, while for Ge–Si alloys, mass-defect scattering could be important. Similarly, in our case the mass difference can be important. Additionally, Tsen et al. [17] reported that the total electron-longitudinal optical phonon scattering rate in GaN is about one order of magnitude larger than that in GaAs. They attributed this enormous increase in the electron-longitudinal optical phonon scattering rate to the much larger ionicity in GaN. In our case, by increasing Mg in our solid solution we increase the

ionicity. Supplementary Hall measurements on the mixed crystals indicate a high carrier concentration; hence, this scattering mechanism cannot be neglected [14].

4 Conclusion

Pyroelectric experiments have proven to be a valuable tool to characterize the thermal parameters of mixed CdMgSe mixed crystals in a limited temperature range around room temperature. The thermal conductivity is found to decrease by a factor of three as the Mg concentration is increased from 0 to about 50 %. This strong variation is attributed to the structural effect of the mixed crystal.

Acknowledgment The authors are indebted to Prof. Mihai Chirtoc for useful advice during the construction of the experimental setup.

References

1. F. Firszt, S. Legowski, H. Męczyńska, H. Oczkowski, W. Osinska, J. Szatkowski, W. Paszkowicz, Z. Spolnik, J. Cryst. Growth **159**, 167 (1996)
2. M.C. Philips, M.W. Wang, J.F. Swenberg, J.O. McCaldin, T.C. Mc Gill, Appl. Phys. Lett. **61**, 1962 (1992)
3. Y. Gou, G. Aizin, Y.C. Chen, L. Zeng, A. Cavus, M.C. Tamargo, Appl. Phys. Lett. **70**, 1351 (1997)
4. F. Firszt, H. Męczyńska, B. Sekulska, J. Szatkowski, W. Paszkowicz, J. Kachniarz, Semicond. Sci. Technol. **10**, 197 (1995)
5. F. Firszt, H. Męczyńska, B. Sekulska, J. Szatkowski, W. Paszkowicz, J. Cryst. Growth **184/185**, 1053 (1998)
6. B.R. Holeman, Infrared Phys. **12**, 125 (1972)
7. A. Mandelis, M. Zver, J. Appl. Phys. **57**, 4421 (1985)
8. M. Rombouts, L. Froyen, A.V. Gusarov, E.H. Bentfour, C. Glorieux, J. App. Phys. **97**, 24905 (2005)
9. M. Chirtoc, G. Mihailescu, Phys. Rev. B **40**, 9606 (1989)
10. A. Salazar, Rev. Sci. Instrum. **74**, 825 (2003)
11. S. Delenclos, M. Chirtoc, A. Hadj Sahraoui, C. Kolinsky, J.M. Buisine, Anal. Sci. **17**, 161 (2001)
12. G. Slack, Phys. Rev. B **6**, 3791 (1972)
13. C.M. Bhandari, D.M. Rowe, *Thermal Conduction in Semiconductors*, 1st edn. (Wiley Eastern Limited, New Delhi, 1998), pp. 59–77
14. K. Perzynska, F. Firszt, S. Legowski, H. Meczynska, J. Szatkowski, M. Biernacka, A. Gajlewicz, S. Tarasenko, P. Zaleski, J. Cryst. Growth **214/215**, 904 (2000)
15. S. Adachi, J. Appl. Phys. **54**, 1844 (1983)
16. B. Abeles, Phys. Rev. **131**, 1906 (1963)
17. K.T. Tsen, D.K. Ferry, A. Botchkarev, B. Sverdlov, A. Salvador, H. Morkoc, Appl. Phys. Lett. **71**, 1852 (1997)